Proceedings of the
Annual Stability Conference
Structural Stability Research Council
Louisville, Kentucky, April 13-16, 2021

Generalized Beam Theory: moving from isolated members to structural systems

Cilmar Basaglia[1], Dinar Camotim[2]

Abstract

This paper presents a state-of-the-art report concerning the most recent Generalized Beam Theory (GBT) formulations and applications developed by authors to assess the buckling behavior of thin-walled steel structural systems. In particular, the paper reports new findings dealing with the use of GBT to analyze (i) locally and globally braced frames, (ii) pitched-roof industrial frames, (iii) roof-supporting trusses and (iv) purlins restrained by sheeting. In each case, the topic or problem under consideration is first outlined, by providing its key features and associated challenges. Then, the main goals of the research effort undertaken are described and followed by a necessarily brief presentation and discussion of the main results/findings obtained. Finally, the paper closes with a few concluding remarks.

1. Introduction

The thin-walled steel structural systems commonly used in the construction industry are very often formed by slender cross-section members (*e.g.*, cold-formed profiles), which invariably exhibit a low torsional stiffness and a high susceptibility to various instability phenomena, namely local, distortional and/or global buckling. This fact explains why assessing the structural response of such systems/structures constitutes a complex task, which requires the performance of either (i) costly and carefully planned experimental tests (*e.g.*, Dubina 2008) or (ii) sophisticated, time-consuming (including data input and result interpretation) and computer-intensive shell finite element analyses (*e.g.*, Jakab 2009, Basaglia *et al.* 2005) − while the latter approach is still prohibitive for routine applications, the former one obviously involves relatively simple structural systems and is restricted to research and validation purposes. In order to render the analysis of thin-walled steel structures computationally simpler and more accessible to practitioners at the preliminary design stages, without sacrificing too much the accuracy of the results obtained, it is mandatory to develop easy-to-use numerical tools based on *beam* finite element models. One very promising route that has been explored in the last two decades is the use of Generalized Beam Theory (GBT).

The GBT, originally aimed at the analysis of prismatic thin-walled *members*, may be described as a beam theory that (i) involves equilibrium equations and boundary conditions expressed in terms of one-dimensional quantities but, nevertheless, (ii) is able to incorporate also folded-plate concepts, making it possible to account for local (wall bending) deformation and cross-section

[1] FEC, DES, University of Campinas, Brazil. <cbasaglia@fec.unicamp.br>
[2] CERIS, DECivil, Instituto Superior Técnico, Universidade de Lisboa, Portugal. <dcamotim@civil.ist.utl.pt>

distortion (*e.g.*, Schardt 1989). The main innovative feature of GBT is the fact that the member cross-section deformation is viewed as a linear combination of "special" shape functions, which are termed "deformation modes" and satisfy a number of orthogonality conditions – this GBT "modal nature" has significant advantages in terms of (i) "structural clarity" of the solution obtained and (ii) computational efficiency. Then, the unknowns appearing in the member equilibrium equations and boundary conditions are functions providing the amplitudes of the contributions of each deformation mode to the deformed configurations of the various cross-sections (*i.e.*, it corresponds to performing "modal decompositions" of the cross-section deformed configurations along the member length). In this context, the authors have recently developed, implemented and validated GBT-based beam finite elements capable of analyzing the local, distortional and global buckling behaviors of thin-walled steel beams, frames and trusses exhibiting localized supports (*e.g.*, those associated with bracing systems) and subjected to arbitrary loading (*e.g.*, Basaglia *et al.* 2009a, Camotim *et al*. 2010, Basaglia *et al*. 2010,2013, Basaglia & Camotim 2011,2013,2015, Camotim & Basaglia 2013,2014, Bebiano *et al.* 2018, da Silva *et al.* 2019).

The main objective of this work is to present and discuss numerical results that illustrate the application, capabilities and potential of the GBT-based beam finite elements mentioned in the previous paragraph. These numerical results concern the buckling behavior of four thin-walled steel structural systems, namely (i) locally and globally braced frames, (ii) pitched-roof industrial frames, (iii) roof-supporting trusses and (iv) purlins restrained by sheeting exhibiting different support conditions and subjected to various loadings. Taking advantage of the GBT unique and structurally clarifying modal features, it is possible to assess how different geometries and/or bracing arrangements affect (improve) the local, distortional and/or global buckling behavior of these structural systems – in particular, the influence of the presence of full or partial displacement restraints, stemming from batten plates (local restraints), tie-rods (global restraints) and purlins/sheeting (natural restraints), can be easily taken into account. The accuracy of the GBT-based buckling results is assessed through the comparison with "exact" solutions, provided by rigorous shell finite element analyses carried out in the commercial code ANSYS (SAS 2013).

2. About Generalized Beam Theory

Since the cross-section displacement field is expressed as a linear combination of structurally meaningful *deformation modes* (of the whole cross-section), GBT analyses involve solving equilibrium equations written in a very convenient and clarifying modal form, leading to solutions that provide in-depth insight on mechanics of the structural response under consideration. Thus, in order to analyze the buckling behavior of a given structure (solution of an eigenvalue problem that yields buckling loads and mode shapes), it is necessary to begin by performing preliminary *cross-section analyses* of all the members (with different cross-sections), which are aimed at (i) identifying the corresponding deformation modes and (ii) evaluating the associated modal mechanical properties − this unique GBT modal decomposition provides the means for a very clear and illuminating interpretation of the structural system buckling behavior.

Consider a prismatic thin-walled member with the (supposedly arbitrary) cross-section depicted in Figure 1, which also shows the local coordinate axes associated with each wall. In order to obtain a displacement field representation compatible with the classical beam theories, in a GBT formulation, the wall mid-plane displacement components $u(x,s)$, $v(x,s)$ and $w(x,s)$ are given by (see Figure 1 and note that s is a coordinate along the cross-section mid-line)

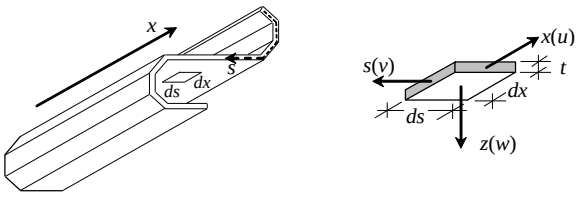

Figure 1: Prismatic thin-walled member with an arbitrary cross-section and wall local coordinate axes (displacement components)

$$u(x,s) = u_k(s)\phi_{k,x}(x) \qquad v(x,s) = v_k(s)\phi_k(x) \qquad w(x,s) = w_k(s)\phi_k(x) \tag{1}$$

where (i) $(.)_{,x} \equiv d(.)/dx$, (ii) the summation convention applies to subscript k, (iii) functions $u_k(s)$, $v_k(s)$, $w_k(s)$, yielded by the *cross-section analysis* (*e.g.*, Bebiano *et al* 2015), characterize deformation mode k and satisfy Vlasov's null membrane shear strain and transverse extension assumptions, and (iv) $\phi_k(x) \equiv \phi_k(X)$ are deformation mode amplitude functions defined along the member length.

Once the deformation modes are known, it is a straightforward matter to establish the member buckling eigenvalue problem, defined by the GBT equilibrium equation system

$$C_{ik}\phi_{k,xxxx} - D_{ik}\phi_{k,xx} + B_{ik}\phi_k - \lambda\left[X^{\sigma}_{jik}\left(W^0_j\phi_{k,x}\right)_{,x} - X^{\tau}_{jki}\left(W^0_{j,x}\phi_k\right)_{,x} + W^0_{j,x}X^{\tau}_{jik}\phi_{k,x}\right] = 0 \tag{2}$$

$$W^0_j = C_{jj}\,\phi^0_{j,xx} \tag{3}$$

where (i) λ is the load parameter (proportional loading is assumed), (ii) C_{ik}, D_{ik} and B_{ik} are cross-section modal mechanical properties (while the C_{ik} and D_{ik} values concern the warping displacements and torsional rotations, the B_{ik} ones stem from the local deformations, *i.e.*, wall bending), (iii) X^{σ}_{jik} and X^{τ}_{jik} are geometric stiffness components associated with the pre-buckling (iii$_1$) normal stress resultants W^0_j (*e.g.*, axial forces or bending moments) and (iii$_2$) shear stresses originating from the longitudinal stress gradients (non-uniform internal forces and moments) – moreover, the concepts and procedures involved in the determination of the differential equilibrium equation are described in Basaglia *et al.* (2010) and Camotim *et al.* (2008, 2010).

3. Thin-Walled Steel Frames

The major difficulty involved in the application of GBT (or any other beam model) to the analysis of thin-walled frames lies in the appropriate handling of the joint behavior. It is indispensable to consider simultaneously (i) the warping transmission stemming from torsional and/or distortional deformations, and (ii) the compatibility between the transverse (membrane and flexural) displacements of the connected member end sections. Moreover it also necessary to be able to simulate the influence of the connections and restraints associated with the presence of bracing systems. In order to overcome the above difficulties, a GBT-based beam finite element approach was developed and numerically implemented, making it possible to assess the first-order and buckling behavior of plane and space thin-walled frames (i) built from open-section or tubular members, (ii) with and without localized supports stemming from bracing systems, (iii) exhibiting various joint configurations and (iv) acted by loadings causing non-uniform internal force and moment diagrams. This work was mostly done by Basaglia *et al.* (2008,2009b,2010, 2015) and fairly complete state-of-the-art reports were published by Camotim *et al.*(2010) and Camotim & Basaglia (2013).

3.1 Locally and Globally Braced Frames

One possible way of improving the frame resistance against the failure prompted by global buckling consists of using diagonal tie-rods (global bracing – see Fig. 2(a)), which transfer part of the horizontal and vertical forces from the members to the frame foundation (*e.g.*, the widespread approach of employing "X" or "V" bracing arrangements in some plane frames). On the other hand, the local critical buckling stress can be increased through the introduction of batten plates (local bracing – see Fig. 2(b)) joining the wall ends of some open cross-sections (*i.e.*, "closing" them) – such battens may be evenly or unevenly spaced along the member length. However, the structural efficiency of these local and global bracing procedures can only be adequately assessed after acquiring in-depth information about the braced frame buckling behaviour, a task involving (i) the identification of the relevant local and global buckling modes and (ii) the evaluation of the associated bifurcation stresses.

Concerning the modelling of the local and global bracing systems, GBT analyses incorporate the rigid tie-rod (global bracing) and batten plates (local bracing) effects by imposing *constraint conditions* (varying from case to case) in the frame stiffness matrices (Basaglia *et al.* 2010). For the inclusion of tie-rods into the analysis, one must impose constraint conditions that ensure the full restraint of the transverse flexural displacement of a member mid-surface point located within a wall (*e.g.*, point *P* in Fig. 2(a)). Concerning the batten plates, these constraints amount to imposing a fixed distance between the flange free ends of the restrained cross-sections (*e.g.*, points A_U^i and A_L^i in Fig. 2(b)) – note that this arrangement restrains only the symmetric local deformation modes [3,4].

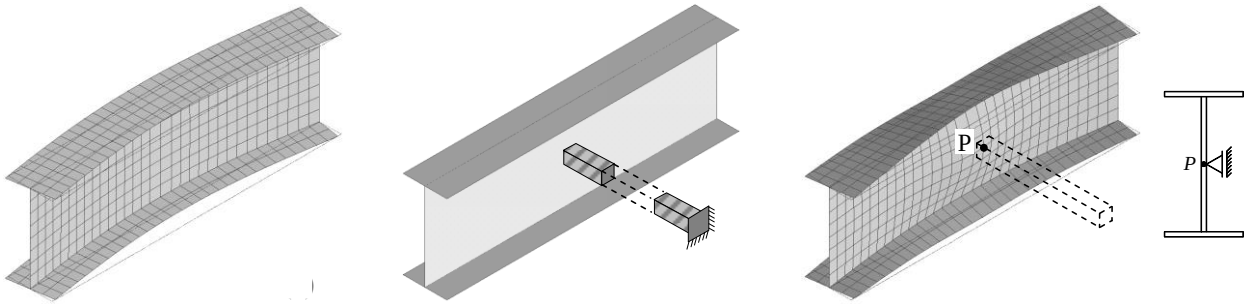

(a)

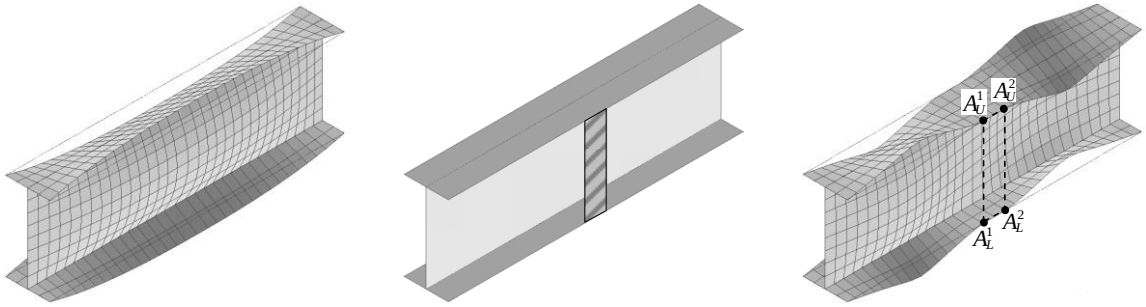

(b)

Figure 2: Member (a) global and (b) local buckling mode shape and bracing details

[3] Increasing the batten plate width amounts to "closing" larger beam segments, thus leading to a much higher bending and (mostly) torsional stiffness values. However, this effect is not accounted for by the GBT analyses, since no restraint is imposed to the corresponding deformation modes.

[4] If the member wall thickness is smaller that the batten plate one, one assumes that the latter exhibits in-plane rigidity.

In this section, one presents and discusses numerical results concerning the assessment of how different bracing arrangements influence the local and global buckling behaviour of the symmetric space frame shown in Figure 3(a) – it comprises two portal frames (*F1* and *F2*) joined by a transverse beam (*TB*) and is acted by five equal vertical loads *P* applied at the four column tops and at the centroid of the transverse beam mid-span cross-section. While all column-to-beam joints are box-stiffened (web continuity), the beam-to-beam joints exhibit flange continuity. As for the support conditions, (i) the column bases are fixed and (ii) the transverse displacements along $\overline{X}$ are prevented at all column-to-beam joints (see Fig. 3(b)). All members have identical cross-sections, with the dimensions given in Figure 4(a), and are made of steel with *E=205 GPa* (Young´s modulus) and *ν=0.3* (Poisson´s ratio). It shows the dimensions and the GBT discretisation adopted (involving natural, end and intermediate nodes). On the basis of this discretisation, the GBT cross-section analysis leads to *15* deformation modes – Figure 4(b) displays the in-plane shapes of the 7 most relevant ones: axial extension (**1**), major/minor axis bending (**2**-**3**), torsion (**4**) and local (**5**-**7**) modes.

One analyses the unbraced frame shown in Figure 4(a) and also frames exhibiting the three bracing arrangements depicted in Figures 5(a)-(c), which are characterised as follows:

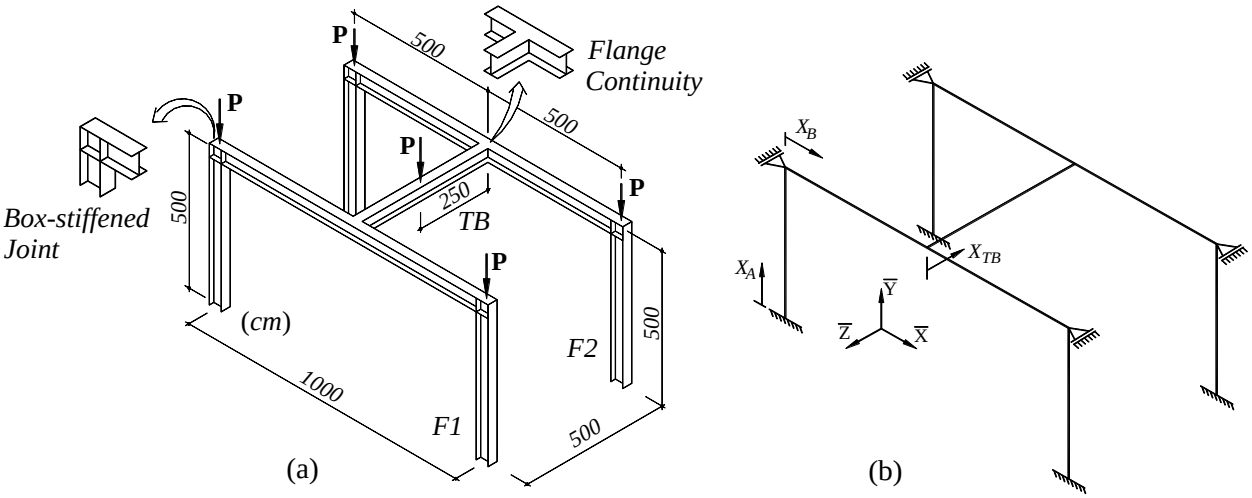

Figure 3: Space frame (a) geometry and loading, and (b) support conditions

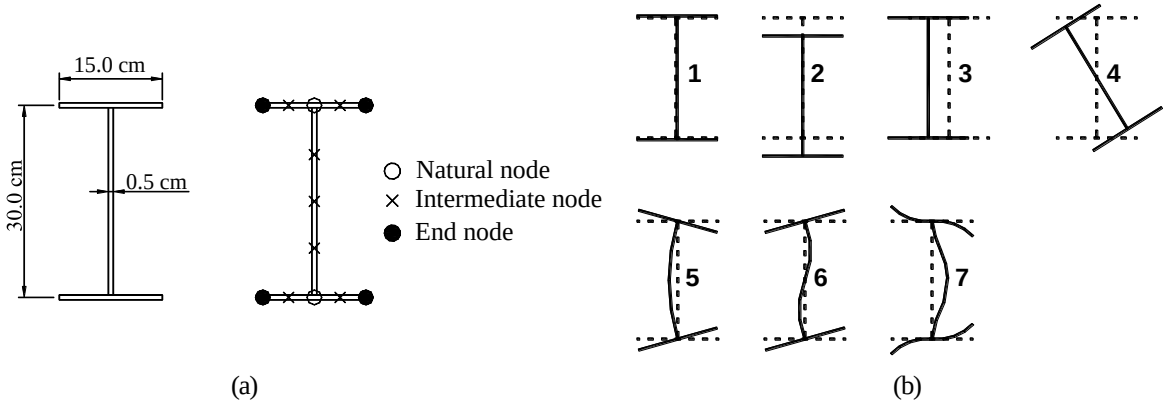

Figure 4: I-section (a) geometry and GBT discretisation, and (b) 7 most relevant deformation mode shapes

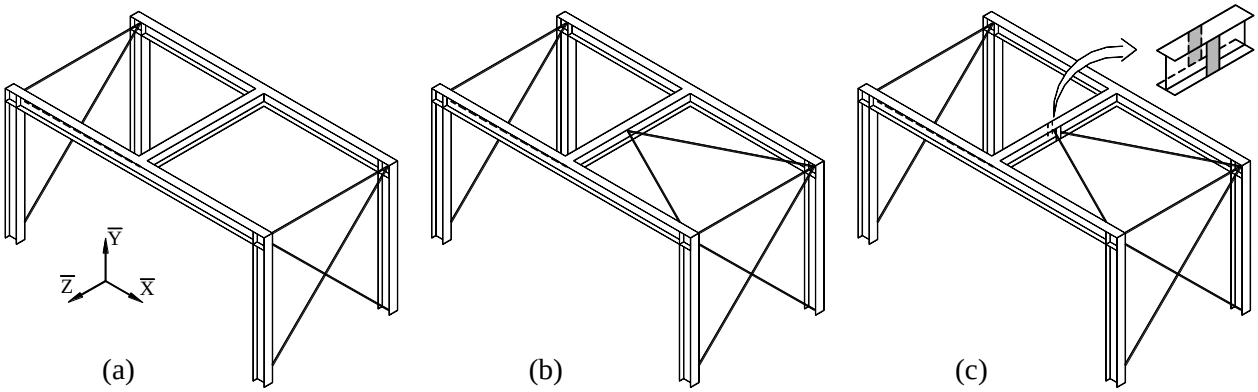

Figure 5: Frame bracing arrangements dealt with in this work: (a) *BR1*, (b) *BR2* and (c) *BR3*

(i) *BR1* – displacements along $\overline{Z}$ prevented at all column-to-beam joints by means of "rigid" tie-rods positioned diagonally (X-configuration) and transversely[5].

(ii) *BR2* – in addition to *BR1*, one also prevents the displacement along $\overline{X}$ at the transverse beam mid-span cross-section, again trough "rigid" tie-rods positioned diagonally (now with a V-configuration).

(iii) *BR3* – in addition to *BR2*, one also uses two batten plates to fix the distance separating the flange free ends at the transverse beam mid-span cross-section.

The buckling results presented (critical loads and mode shapes) are obtained by means of (i) the GBT beam finite element formulation briefly described earlier and also (ii) shell finite element analyses carried out in ANSYS (SAS 2013), adopting frame and bracing discretisations into fine meshes of SHELL181 and BEAM189 elements (ANSYS nomenclature)[6].

While Table 1 shows the frame GBT and ANSYS critical loads concerning the braced and unbraced frames, Figures 6 to 9 provide two representations of the corresponding buckling mode shapes, namely (i) 3D-views yielded by the ANSYS analyses and (ii) the amplitude functions of the GBT deformation modes. At this stage, it is worth noting that the GBT analyses were based on frame discretisations involving *80* finite elements (*8* per column and *16* per beam), which corresponds to *1030* degrees of freedom – their ANSYS counterparts require the consideration of more than *25000* degrees of freedom.

The observation of the results shown in Table 1 and Figures 6 to 9 prompts the following remarks:

Table 1: GBT and ANSYS frame critical loads (kN)

Frame		GBT	ANSYS	Δ(%)
Unbraced		43.25	44.19	-2.13
Braced	*BR1*	73.25	74.13	-1.19
	BR2	161.83	159.11	1.71
	BR3	167.33	167.42	-0.05

[5] All tie-rods are connected to the corresponding member cross-section mid-web points.

[6] The tie-rod and batten plate modelled exhibited (i) a *6cm* square cross-section and (ii) *30×7.5×0.7cm* dimensions, respectively.

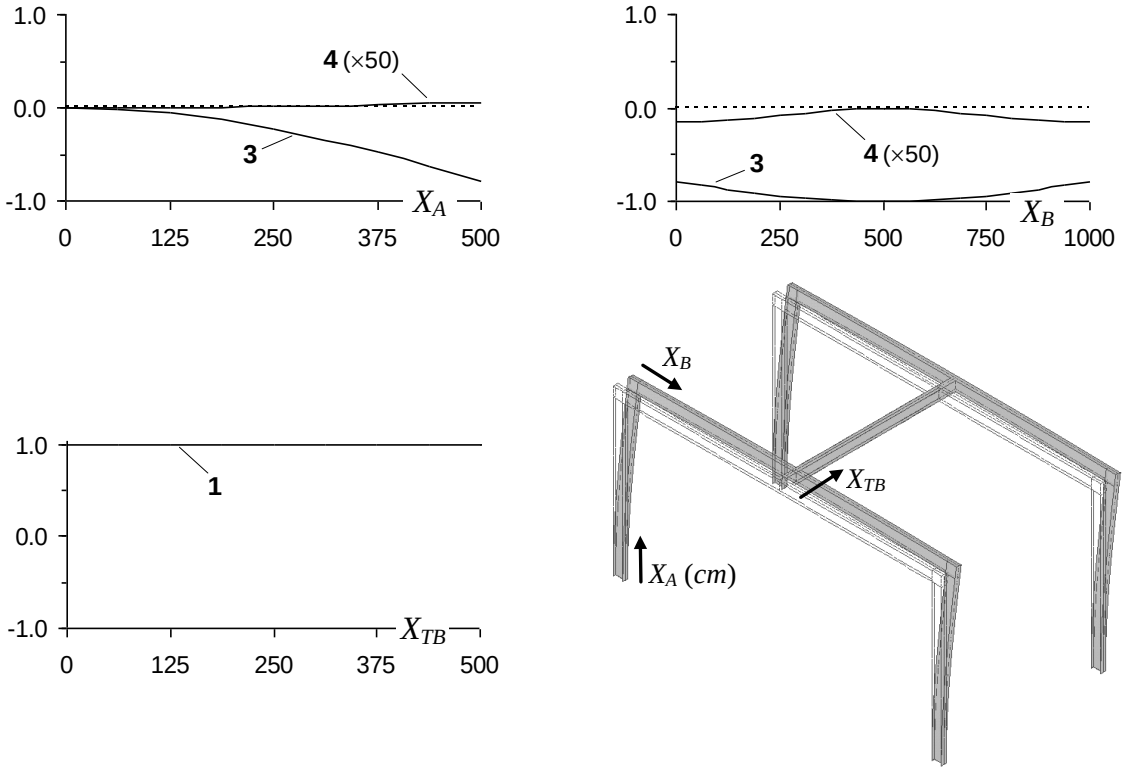

Figure 6: Unbraced frame – GBT and ANSYS critical buckling mode representations

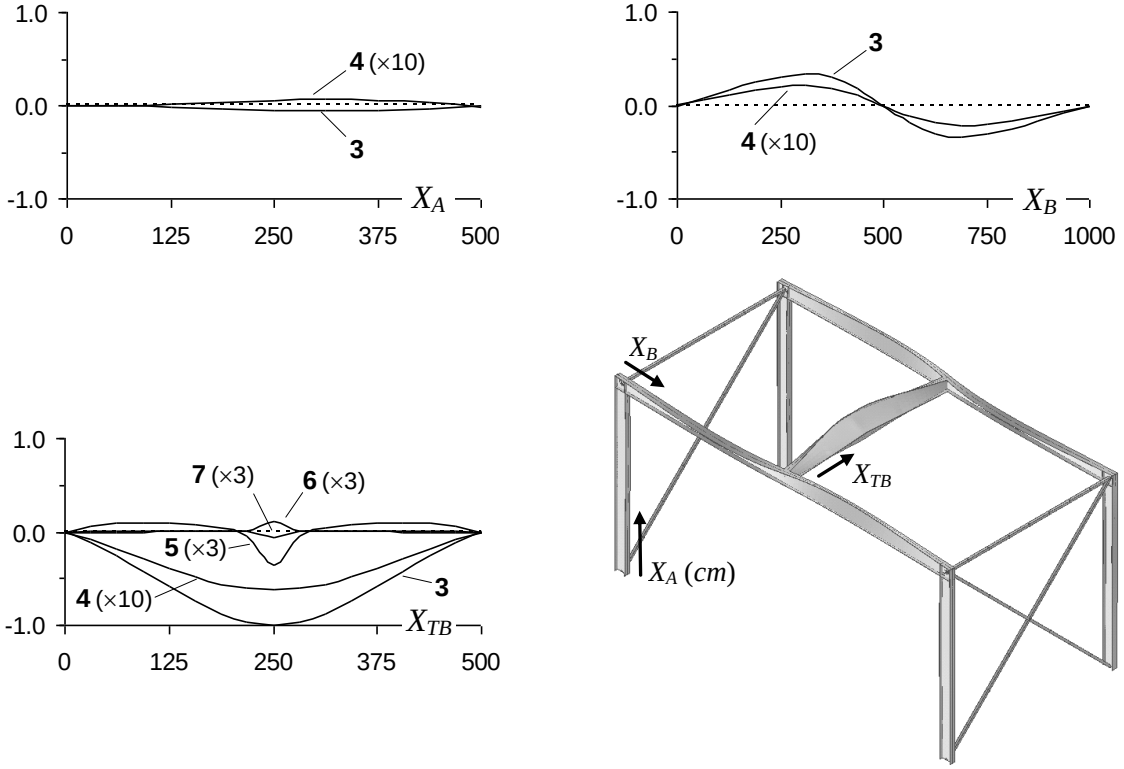

Figure 7: *BR1* braced frame – GBT and ANSYS critical buckling mode representations

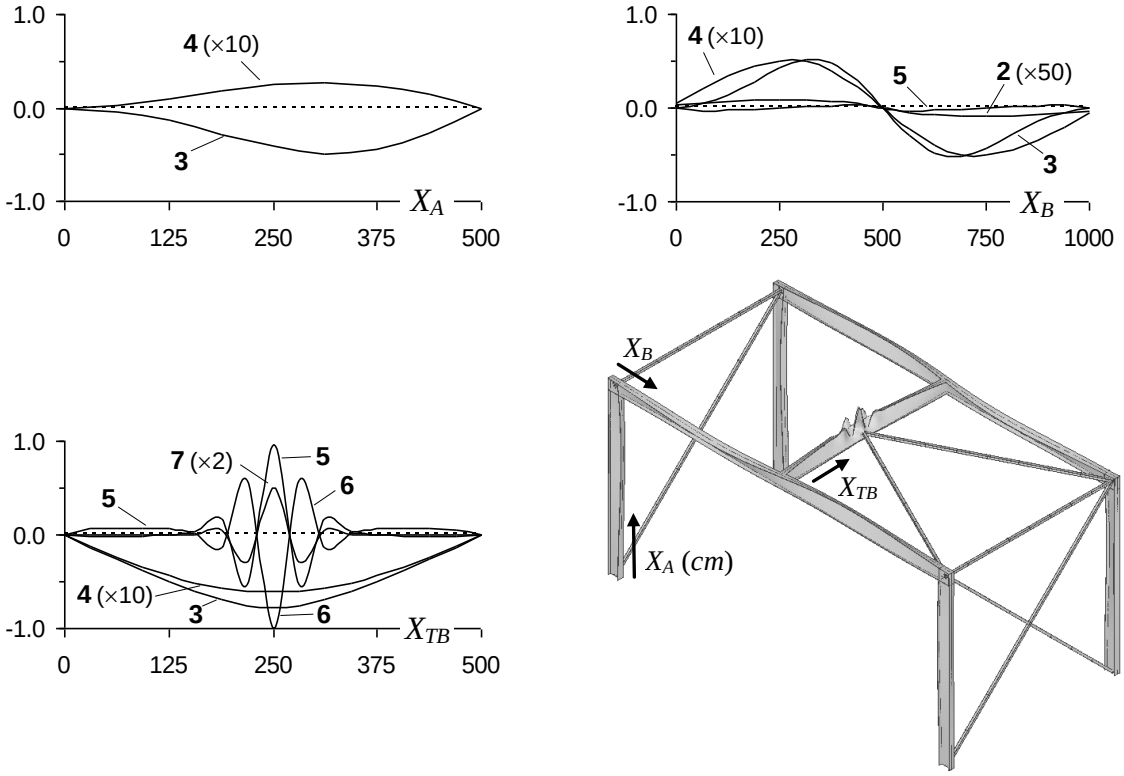

Figure 8: *BR2* braced frame – GBT and ANSYS critical buckling mode representations

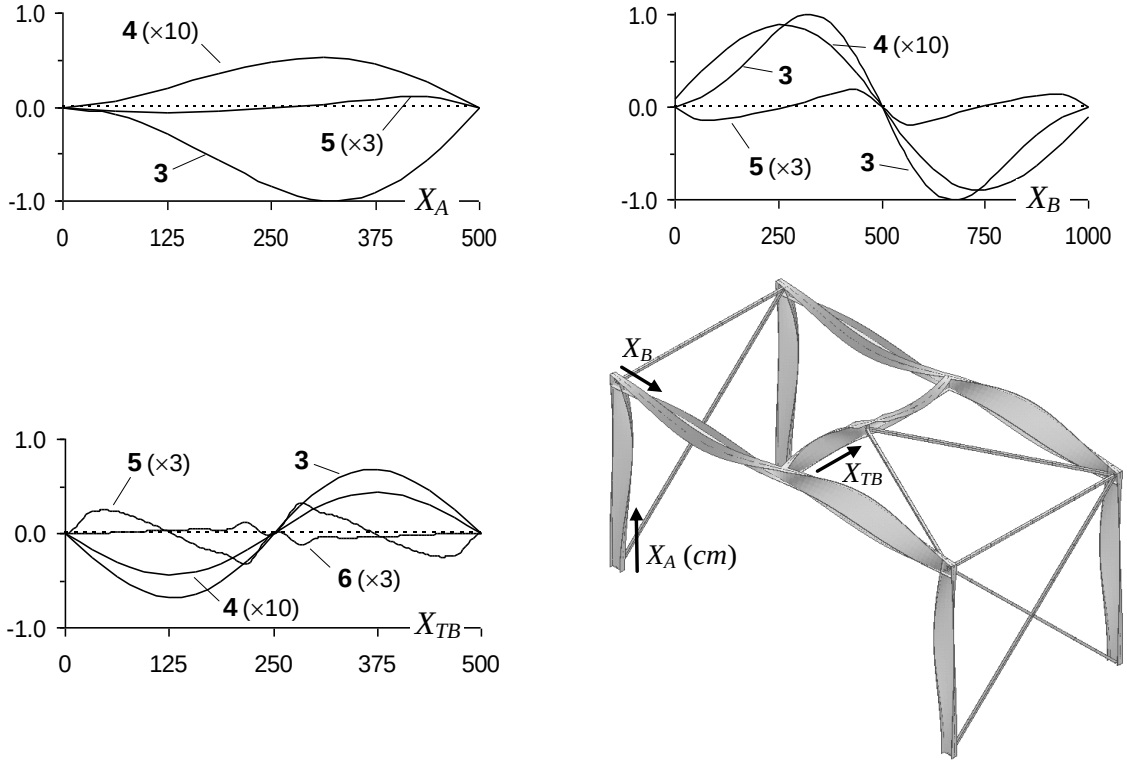

Figure 9: *BR3* braced frame – GBT and ANSYS critical buckling mode representations

(i) First of all, there is a virtual coincidence between the critical loads yielded by the GBT and ANSYS finite element analyses (all differences below *2.2%*). Moreover, there is also very close agreement between the buckling mode shapes provided by ANSYS analyses and the GBT modal amplitude functions – however, the latter representations provide a deeper insight on the mechanics of frame buckling, as well as on the influence of the bracing arrangement.

(ii) Table 1 shows that the presence of the bracing arrangements leads to critical buckling load increases amounting to *69%* (*BR1*), *274%* (*BR2*) and *287%* (*BR3*).

(iii) The unbraced frame critical buckling mode involves mainly minor axis bending displacements (mode **3**) of the portal frames and axial translation of the transverse beam, together with lateral motions of all frame joints. Therefore, it is clear that restraining the lateral motions of the joints will enhance the frame buckling resistance.

(iv) The *BR1* braced frame critical buckling mode combines global (flexural-torsional) and local deformation modes. The former, which are clearly dominant, consist of (iv_1) a major contribution from mode **3** (minor axis bending) and (iv_2) a relevant participation of mode **4** (torsion)[7]. In addition, there are also non-negligible contributions from the local modes **5**, **6** and **7** in the vicinity of the transverse beam mid-span cross-section. Since buckling is clearly triggered by the transverse beam lateral-torsional instability, the frame resistance can be increased by preventing its the mid-span lateral displacement (global bracing).

(v) The *BR2* braced frame critical buckling mode is triggered by the transverse beam and combines participations of both global (**3** and **4**) and local (**5**, **6** and **7**) deformation modes − while the latter occur mainly in the beam mid-span region (higher bending moments), the influence of the former is felt along the whole beam length. A further improvement of the frame buckling resistance can be achieved by reducing the beam local deformations.

(vi) The *BR3* braced frame buckles in a mode that involves very small local deformations in the transverse beam. Indeed, the frame critical buckling is predominantly associated with the lateral-torsional behavior of all members (modes **3** and **4**) – due to the mid-span local bracing, the transverse beam exhibits now two half-waves. The major contribution to the frame buckling mode comes from mode **3**, with similar maximum values occurring at the portal frame columns and beams.

3.2 Pitched-Roof Industrial Frames

Next, the above GBT-based beam finite element approach is used to assess how the purlin restraints affect the buckling behaviour of the pitched-roof steel frame depicted in Figure 10(a). The frame (i) is built from identical I-section members (web height *300mm*, flange width *150mm* and wall thickness *6.35mm* – see Fig. 11), (ii) is acted by identical evenly spaced vertical loads *Q*, transferred directly to the rafters by the purlins, and (iii) has box-stiffened column-rafter joints and a diagonal-stiffened apex joint (see Fig. 10(b)). Moreover, (i) the column bases are fixed and (ii) the out-of-plane transverse displacements are prevented at the joints and column mid-heights (restraints deemed localized at the cross-section centroids/shear centres – *e.g.*, see the column restraint shown in Fig. 10(c)).

In the GBT-based analysis of plane frames, the influence of the lateral displacement partial restraints provided by the purlin/sheeting systems to the rafters may be modelled by means of elastic supports (translational springs of stiffness κ), evenly spaced along the rafter top flanges and located at the purlin centroidal (longitudinal) positions – see Figure 11. The additional stiffness associated with

[7] Note that the GBT normalisation procedure adopted renders the mode **4** amplitude function "artificially small".

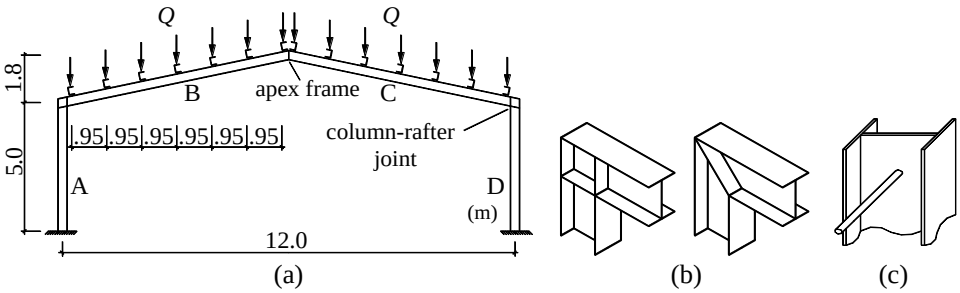

Figure 10: (a) Frame geometry and loading, (b) box-stiffened and diagonal stiffened joints, and (c) column localised support

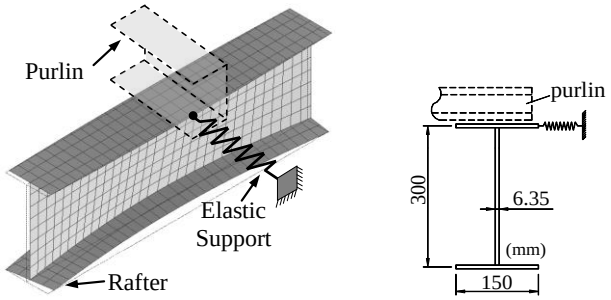

Figure 11: Modelling of the elastic lateral displacement restraints provided by the purlin/sheeting system to the rafter

these elastic supports/springs must be incorporated into the frame overall stiffness matrix (*e.g.*, Camotim *et al*. 2008) and it is worth noting that the displacement restraints involve exclusively the rafter minor-axis bending (mode **3**) and torsion (mode **4**) behaviours.

The curve displayed in Figure 12(a), obtained by means of GBT buckling analyses, provides the variation of the frame critical load (Q_{cr}) with the lateral restraint stiffness κ – the circles correspond to values yielded by ANSYS shell finite element analyses. For selected κ values, Figure 12(b) shows the GBT-based top flange lateral displacement profiles v concerning rafter B and corresponding to the critical buckling mode – note that all displacements v are obtained by means of the second of Eqs. (1) and normalized with respect to the maximum value, occurring for $\kappa=0$ and $X_B=321.04cm$. Finally, Figures 13 and 14 display critical buckling mode representations of (i) the unrestrained frame (κ=0) and (ii) a laterally restrained frame with $\kappa=20kN/cm$: a 3-D overall view yielded by ANSYS and GBT-based deformation mode amplitude functions concerning column *A* and rafter *B*. The observation of these buckling results leads to the following remarks:

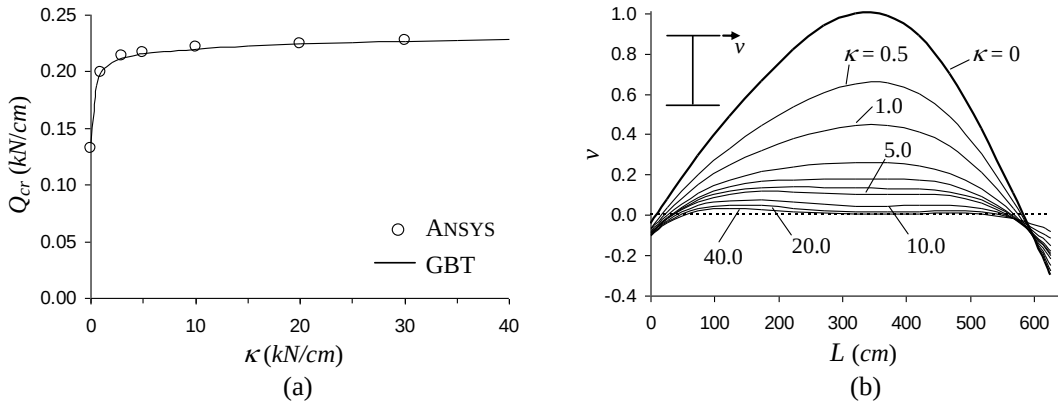

Figure 12: (a) Frame critical load *vs.* lateral restraint stiffness and (b) rafter B top flange lateral displacement profiles

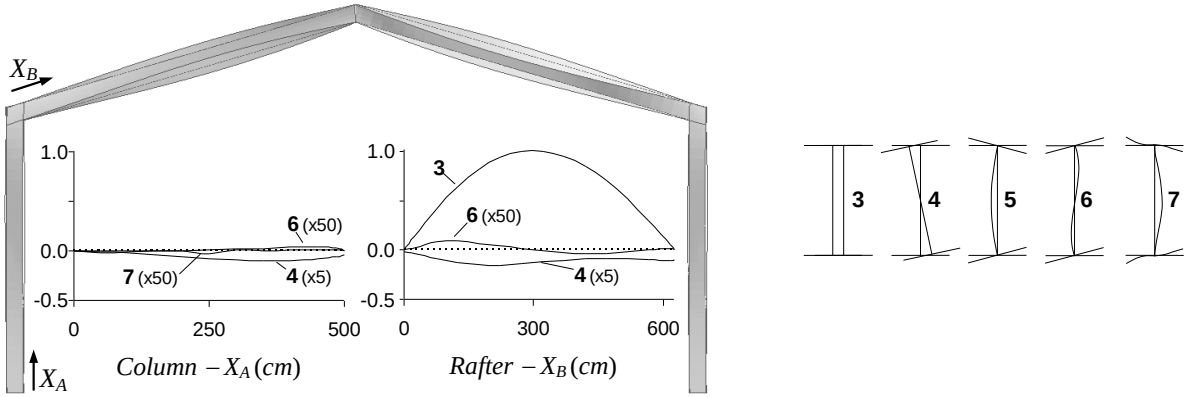

Figure 13: ANSYS and GBT critical buckling mode of the unrestrained frame (κ=*0*)

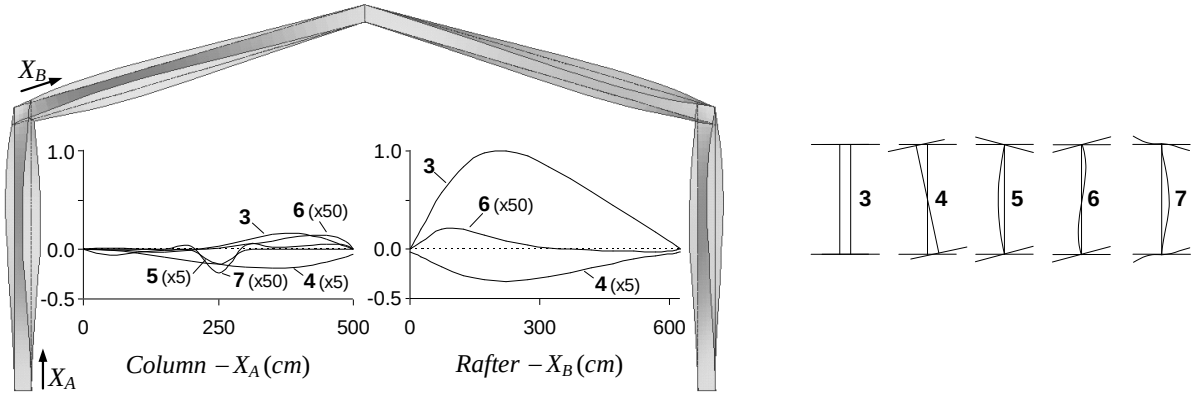

Figure 14: ANSYS and GBT critical buckling mode of the laterally restrained frame with κ=*20 kN/cm*

(i) The GBT and ANSYS critical buckling loads (all differences below *3.0%*) and mode shapes virtually coincide. Note that the numbers of degrees of freedom involved in the two analyses are orders of magnitude apart: *660* (GBT – *50* beam finite elements: *15* per rafter and *10* per column) versus *13000* (ANSYS).

(ii) The lateral restraints cause a critical load increase value reaching *66%*, for κ=*40kN/cm*. However, note that this increase is significant even for rather low stiffness values (*e.g.*, κ=*0.5kN/cm* leads to a *37%* Q_{cr} increase). These results show how beneficial would be to be able to account for the lateral restraints stemming from the purlin/sheeting system in the frame buckling analysis and design procedure, particularly since the rafters are often quite long and acted by considerable compressive loads, *i.e.*, highly prone to instability. The major hurdle preventing the incorporation of this effect into the frame analysis/design lies in the lack of a fairly simple and reliable methodology to predict the actual lateral restraint stiffness.

(iii) Figure 12 (b) shows how increasing the lateral restraint stiffness lowers and changes the profile of the rafter upper flange lateral displacements – note that they become progressively "more constant" along a growing rafter central region.

(iv) Figures 13 and 14 make it possible to visualise how the lateral restraints influence the buckling mode shape. While the unrestrained frame buckling is almost exclusively triggered by the rafter lateral-torsional instability, the restrained frame (κ=*20kN/cm*) buckles in a mode that clearly exhibits non-negligible contributions from column local and global deformations.

4. Thin-Walled Roof-Supporting Trusses

The thin-walled steel trusses commonly used in the construction industry to support roof structures are frequently built from open-section members with their end sections connected through pinned joint arrangements (often consisting of bolts joining the webs and/or flanges). These structural systems are currently designed by means of indirect methods, based on individual member safety checks that adopt "effective width" concepts to account for local and distortional buckling effects.

Accurate analyses of thin-walled steel trusses will only be useful to designers if they are complemented with an easy access to fast and user-friendly numerical tools to perform them. Such numerical tools must necessarily be based on *beam* finite elements that (i) account for local and distortional buckling effects, and (ii) can handle the pinned joint displacement compatibility. In this context, the authors have very recently improved an existing GBT-based beam finite element approach, making it capable analyzing the local, distortional and global buckling behavior of plane thin-walled steel trusses built from open cross-section members and having various joint configurations (Basaglia & Camotim 2011,2015). This approach includes (i) a "joint element" concept, relating the connected member GBT degrees of freedom to the joint generalized displacements, and (ii) *constraint conditions* ensuring local and distortional displacement compatibility at the truss joints.

In order to illustrate the application and capabilities of the above improved GBT-based beam finite element approach, numerical results concerning the local and global buckling behavior of simple plane trusses with the geometry depicted in Figure 15 are presented and discussed next. The trusses are (i) formed by two chords (U100×50×3.0 cross-section) and two diagonals (U90×45×1.7), all subjected to (in-plane) minor axis bending, and (ii) acted by two equal vertical loads *P* applied at the upper chord-diagonal joints – all truss and cross-section dimensions are given in Figures 15 and 16(a), respectively. Figure 16(b) shows the in-plane shapes of the *8* GBT deformation modes that play relevant roles in the truss buckling behaviors considered in this work.

Two different truss heights are considered, namely *h=700mm* (short truss) and *h=1050mm* (tall truss). In both cases, (i) the chords have locally and globally pin-ended supports with free warping, and (ii) the diagonals are connected to the chords through bolt pairs with a common axis that passes through

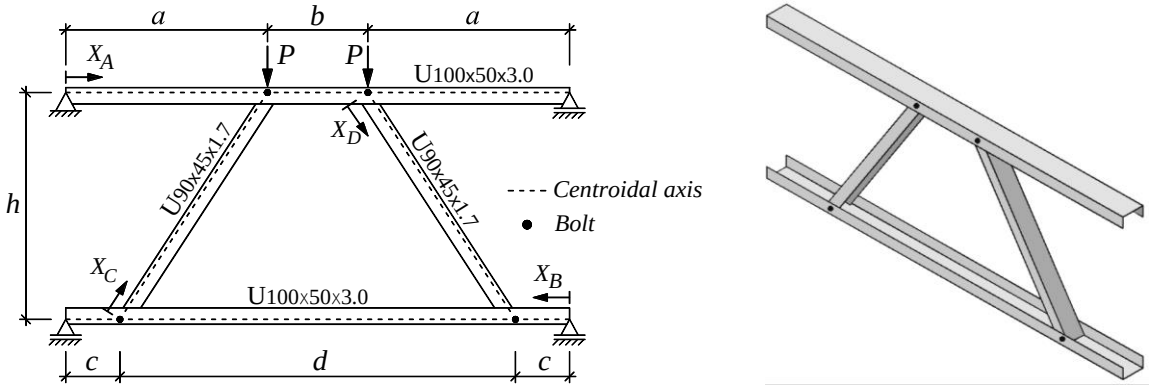

Truss	*h* (*mm*)	*a* (*mm*)	*b* (*mm*)	*c* (*mm*)	*d* (*mm*)
Short	*700*	*750*	*300*	*300*	*1200*
Tall	*1050*			*75*	*1650*

Figure 15: Plane truss schematic representation, three-dimensional view and member dimensions (short and tall trusses)

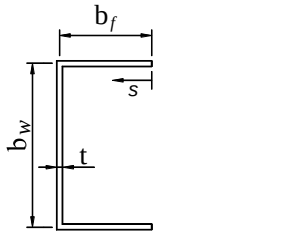

Designation	b_w (mm)	b_f (mm)	t (mm)
U100×50×3.0	100	50	3.0
U90×45×1.7	90	45	1.7

(a)

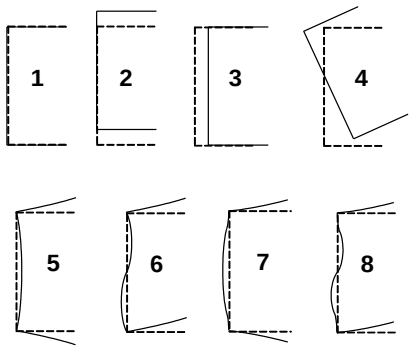

(b)

Figure 16: Plain channel section (a) geometry and GBT discretisation, and (b) in-plane shapes of the *8* most relevant deformation modes

their cross-section centroids. Figure 17(a) shows in detail a diagonal-chord joint: the bolts connect the flange points *P* and *P'*, where the joint is deemed materialized (see Fig. 17(b)), and the two members may then rotate freely about the common bolt axis. In order to ensure displacement compatibility in this joint configuration, (i) a "joint element" is placed at mid-height between the two bolts and (ii) *constraints conditions* Π_P and $\Pi_{P'}$ are enforced. These conditions (i) concern the equality between the transverse bending displacements at the bolted region, (ii) involve mid-surface points P_A, P_B, P'_A, P'_B and (iii) read

$$\Pi_P = \sum_{k=5}^{n} w_k(_{P_A})\phi_k(x_{P_A}) - \sum_{k=5}^{n} w_k(_{P_B})\phi_k(x_{P_B}) = 0$$

$$\Pi_{P'} = \sum_{k=5}^{n} w_k(_{P'_A})\phi_k(x_{P'_A}) - \sum_{k=5}^{n} w_k(_{P'_B})\phi_k(x_{P'_B}) = 0 \qquad (4)$$

It is worth noting an obvious limitation of this approach: the constraint condition model does not take into account the effects related to the surface contact between the connected flanges.

Once all member support and joint compatibility conditions are enforced, the truss linear $[\tilde{K}]$ and geometric $[\tilde{G}]$ stiffness matrices can be readily expressed in terms of "*mixed*" d.o.f. (GBT modal and "conventional" nodal d.o.f. – *e.g.*, Basaglia *et al.* 2009b, Camotim *et al.* 2010, Basaglia & Camotim 2011). Then, the joint compatibility is incorporated into the truss overall stiffness matrix through

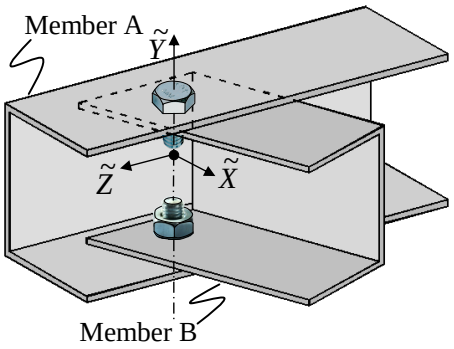

(a)

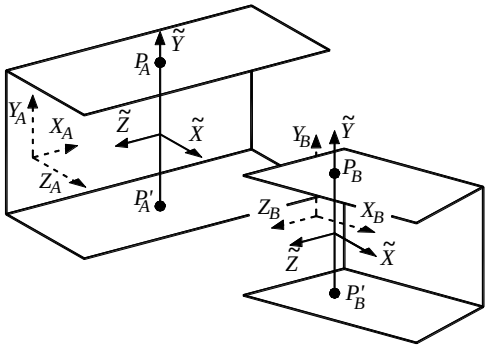

(b)

Figure 17: (a) Truss joint connecting plain channel members and (b) nodes where the joint is deemed materialized

$$([\widetilde{K}]+\lambda[\widetilde{G}])=[\Omega]^T([K]+\lambda[G])[\Omega] \tag{5}$$

where (i) λ is the *load parameter*, (ii) the tilde (~) identifies the stiffness matrices including the joint compatibility conditions and (iii) the compatibility matrix [Ω], defined by

$$\{d\}=[\Omega]\{\widetilde{d}\} \tag{6}$$

contains the joint modal displacement values (*e.g.*, $w_k(P_A), w_k(P_B), w_k(P'_A), w_k(P'_B)$) – $\{d\}$ is the GBT degree of freedom vector and $\{\widetilde{d}\}$ is the vector that already includes the joint compatibility conditions. Once the truss total stiffness matrix ($[\widetilde{K}]+\lambda[\widetilde{G}]$) is known, it is necessary (i) to solve the buckling eigenvalue problem is solved and (ii) to transform the nodal d.o.f. back into GBT ones, through the operation defined in (6).

As before, the buckling results provided by the GBT approach are compared with the values yielded by ANSYS shell finite element analyses, in which (i) the truss members are discretised into fine meshes of SHELL181 elements and (ii) the bolted pinned joints are modelled by coupling the degrees of freedom associated with the translations of the bolted flange nodes.

In both trusses, the maximum compressive axial force and minor-axis bending moment occur in the diagonals and lower chord, respectively – see Figure 18. While the former is more relevant in the tall truss (*25%* higher than in the short truss), the latter prevails in the short truss (about three times higher than in the tall truss). Therefore, the instabilities of the short and tall trusses are triggered by (i) the lower chord local buckling and (ii) the diagonal global (flexural-torsional) buckling, respectively. Indeed, the two truss geometries were selected to enable showing that the GBT analysis is able to capture accurately both local and global buckling phenomena.

Figures 19 (a)-(b) and 20 (a)-(b) show two critical buckling mode representations of the short and tall trusses. While the former are 3D views yielded by ANSYS shell finite element analyses, the latter consist of functions providing the variation of the GBT deformation mode amplitudes along the various truss member lengths. It is worth mentioning that the GBT analyses (i) include *10* deformation modes (the in-plane shapes of *8* of them are depicted in Fig. 16(b)) and (ii) are based on truss longitudinal

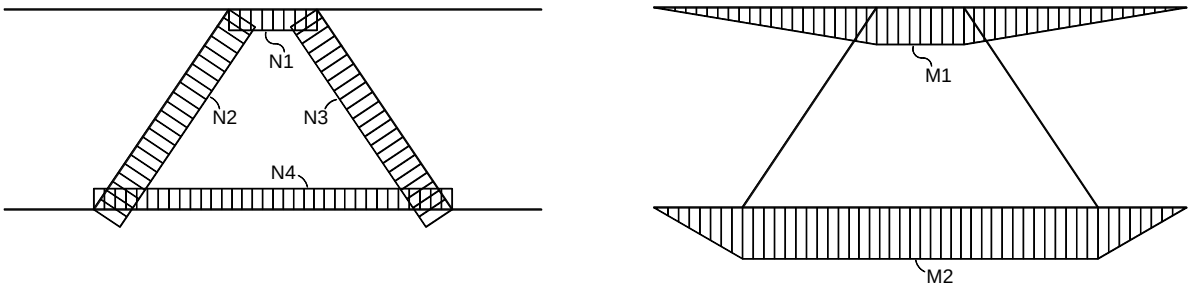

Axial Force — Minor-axis bending moment

Truss	N1	N2	N3	N4	M1	M2
	(kN)				(kNcm)	
Short	*– 0.50*	*– 0.93*	*– 0.93*	*+ 0.50*	*16.53*	*23.39*
Tall	*– 0.63*	*– 1.16*	*– 1.16*	*+ 0.63*	*1.88*	*7.32*

Figure 18: Axial force and bending moment diagrams of the short and tall trusses

discretisations into *82* finite elements (*18* in the upper chord, *40* in the lower chord and *12* in each diagonal), which amounts to a total of *1720* degrees of freedom. On the other hand, the ANSYS shell finite element model involves more than *43700* (short truss) and *50600* (tall truss) degrees of freedom. Although no special effort was made to minimise the ANSYS degree of freedom numbers, they are once more orders of magnitude apart from those required to perform the GBT analyses – which, in addition, provide in-depth insight on the truss buckling mechanics. The observation of the critical buckling loads and mode shapes provided by the GBT and ANSYS analyses, as well as the comparison between them, prompts the following remarks:

(i) First of all, there is an excellent agreement between the two critical load pairs. Indeed, one has (i_1) $P_{cr.GBT}=16.23kN$ and $P_{cr.ANSYS}=16.04kN$ (*1.2%* difference), for the short truss, and (i_2) $P_{cr.GBT}=46.57kN$ and $P_{cr.ANSYS}=44.92kN$ (*3.7%* difference), for the tall truss.

(ii) There is also a rather close agreement between the two critical buckling mode representations displayed in Figures 19 and 20. However, the GBT deformation mode amplitude functions provide again a structural insight that would be virtually impossible to obtain through the shell finite element results – *e.g.*, the amount and nature of the local deformation involved in the buckled joint region can be readily assessed by merely looking at Figures 20 (a)-(b).

(iii) While only symmetric local deformation modes (**5** and **7**) have visible contributions to the short truss buckling mode, the tall truss buckling mode involves both global (major axis flexure and torsion – **2** and **4**) and anti-symmetric local (**6** and **8**) deformation modes.

(iv) In the short truss, the instability is triggered by the local buckling of the lower chord span comprised between the two diagonals, which is subjected to high sagging moments. Since only the flange tips are under compression, buckling involves mainly the flanges and barely occurs in the web. The GBT deformation mode amplitude functions reflect this fact, as the contributions from the symmetric modes **5** and **7** (iv_1) oppose each other in the web and (iv_2) reinforce each other in the flanges – see Figures 16(b) and 20(a).

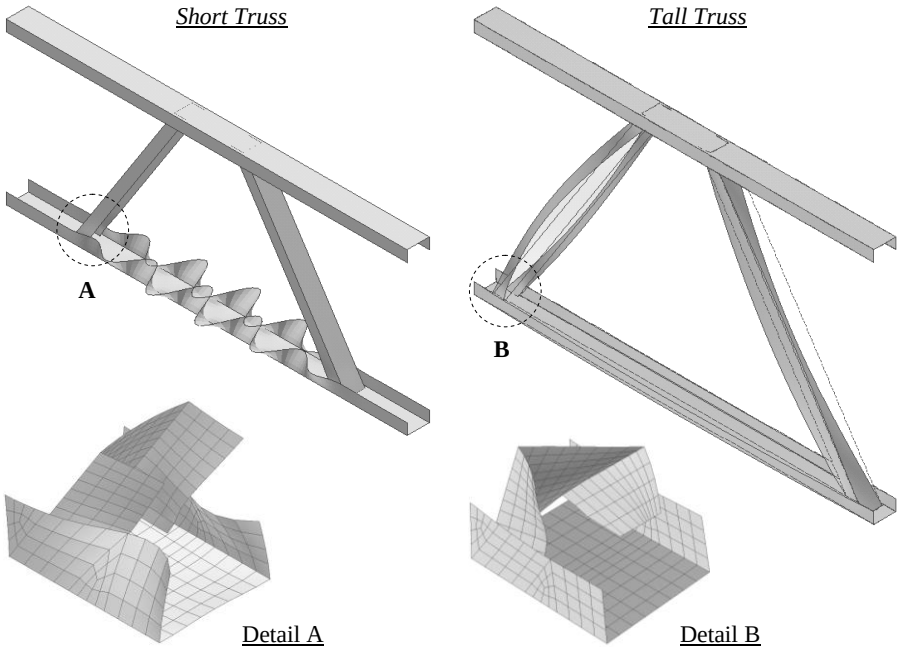

Figure 19: (a) Short truss and (b) tall truss ANSYS critical buckling mode shapes and enlarged lower chord/diagonal joints

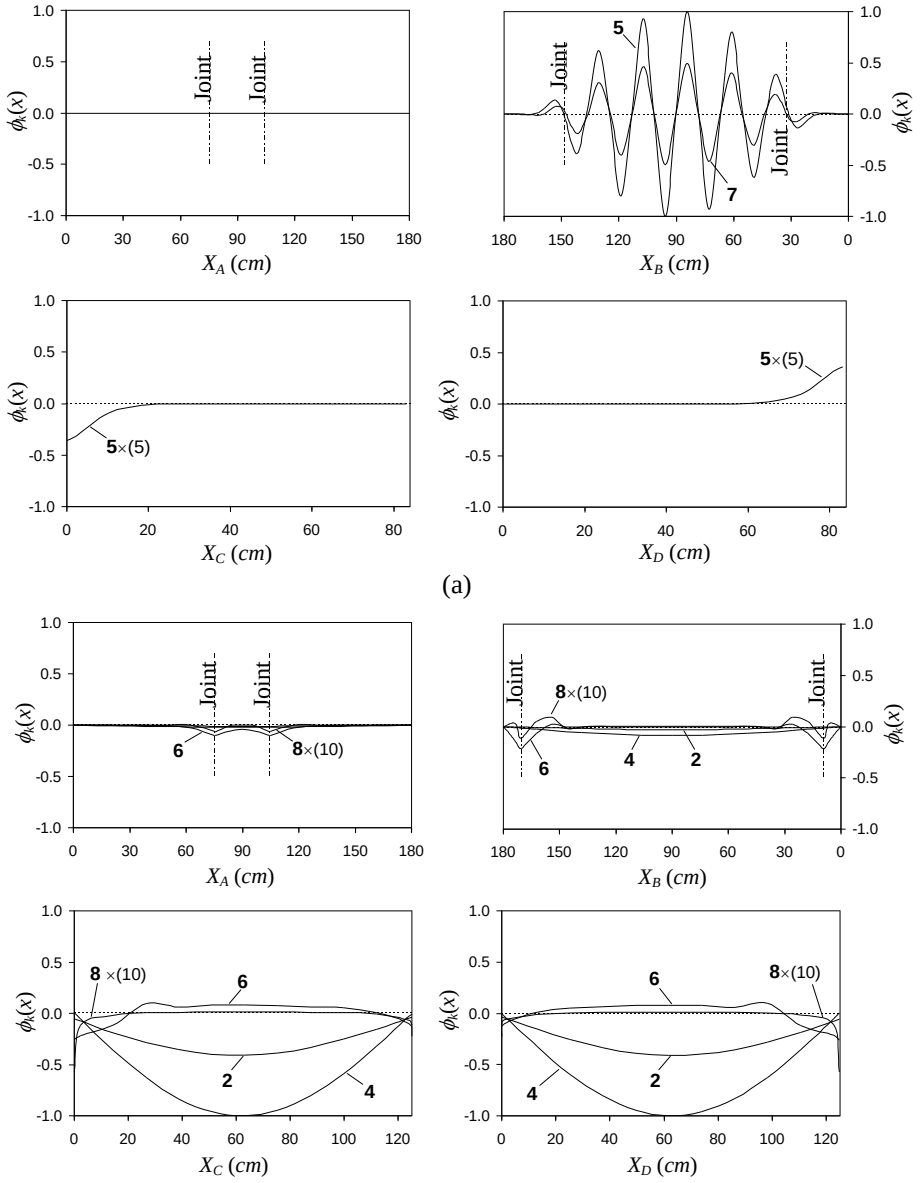

(a)

(b)

Figure 20: (a) Short truss and (b) tall truss: member deformation mode amplitude functions $\phi_k(X)$

(v) In the tall truss, instability is triggered by the global (flexural-torsional) buckling of the two highly compressed diagonals. There is a major contribution from mode **4** and also a relevant participation from mode **2** (both with maximum values at the diagonal mid-spans). The local deformations, associated with the participations of the anti-symmetric modes **6** and **8**, are restricted to the (upper and lower) chord and diagonal regions in the close vicinity of the joints. The anti-symmetric nature of this local deformation stems from the diagonal torsion, which "forces" the chord (mostly) and diagonal flanges to rotate in the same direction near the joints, thus causing double curvature bending in the webs – recall the shapes of modes **6** and **8**, which are shown in Figure 16(b).

(vi) In both trusses, the upper chord plays virtually no role in the buckling mechanics. Indeed, its deformations are either null (short truss) or restricted to the joint close vicinity (tall truss).

5. Purlins Restrained by Sheeting

The last decades have witnessed a significant reduction in the use of heavy sheeting in industrial buildings (*e.g.*, fiber cement roof sheets), as they have been increasingly replaced by lighter sheeting, such as cold-formed steel sheeting, which is more cost-efficient and easier/quicker to construct/erect (*e.g.*, Davies 1991). This is because the hook bolts, previously used to connect the roof sheeting to the cold-formed steel purlins, have been gradually replaced by self-drilling screws, which lead to a higher structural efficiency of the purlin-sheeting assembly (*e.g.*, Tomà *et al.* 1993) – see Figure 21(a). Thus, it is economically advantageous (and makes full structural sense) to base the purlin design on the joint behavior of the whole purlin-sheeting assembly, instead of adopting the traditional approach of viewing the purlins as independent/isolated members. For instance, in the case of purlins subjected to uplift loading, the sheeting restraint changes the buckling mode nature from lateral-torsional to lateral-distortional, as shown in Figure 21(b).

The structural efficiency of open-section thin-walled steel purlins connected to roof sheeting and acted by wind uplift can only be adequately assessed after acquiring in-depth information on the mechanics of its buckling behavior, a task involving (i) the identification of the relevant buckling modes and (ii) the calculation of the associated critical buckling (bifurcation) stresses. However, since these purlins (i) are continuously restrained along their lengths by the roof sheeting, both laterally and torsionally and (ii) display very slender cross-sections, making them highly susceptible to local, distortional and global instability phenomena, the assessment of their structural response constitutes a very complex task. In order to incorporate such (elastic) restraints in a GBT analysis, two approaches can be followed: (i) incorporate the restraints in the cross-section analysis, taking them into account at the deformation mode determination stage (Schardt 1989 and Jiang & Davies 1997 adopted this approach for global and very specific distortional deformations) or (ii) include the restraints only in the member analysis, as constraint equations, which means that the deformation modes are calculated without considering the restraints (Camotim *et al.* 2008, Basaglia *et al.* 2013 and Bebiano *et al.* 2018, authors of the code GBTUL2.0, adopted this approach for arbitrary deformation patterns, which amounts to combining the conventional deformation modes at the member analysis stage. This last approach requires larger deformation mode sets and it may be argued that it somewhat "clouds" the structural interpretation of the results. However, the authors have recently developed and numerically implemented a novel GBT formulation for the local, distortional and global buckling analysis of thin-walled restrained members, based on a cross-section analysis procedure that incorporates elastic restraints and, therefore, is capable of providing accurate buckling results with only a few deformation modes (*e.g.*, da Silva *et al.* 2019).

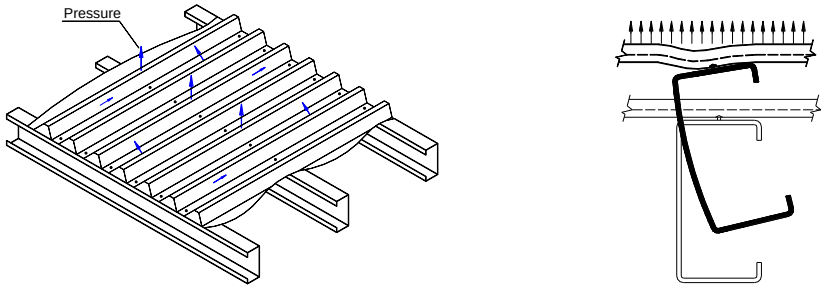

(a) (b)

Figure 21: (a) Lipped channel purlin restrained by roof sheeting and (b) Lateral-distortional buckling mode configuration of purlin subjected to an uplift uniformly distributed load

5.1 GBT Formulation

The modelling of the restraint provided by the sheeting to the member involves continuous translational and rotational elastic springs, which restrain the member transverse displacements and mid-width rotations. Figure 22(a) illustrates the case of a purlin-sheeting assembly: to simulate the restraint provided by the roof sheeting, continuous translational and rotational elastic springs (stiffness K_T and K_R, respectively) are continuously attached to the upper flange mid-points along the whole purlin length. As far as Figure 22(b) is concerned, deals with a prismatic thin-walled open cross-section member, formed by n distinct plate/wall elements, and restrained by continuous translational and rotational elastic springs, located, respectively, at points P_T and P_R, where x, s and z are local coordinates along the member axis, cross-section mid-line and wall thickness, thus leading to member mid-surface displacement components $u(x,s)$, $v(x,s)$ and $w(x,s)$.

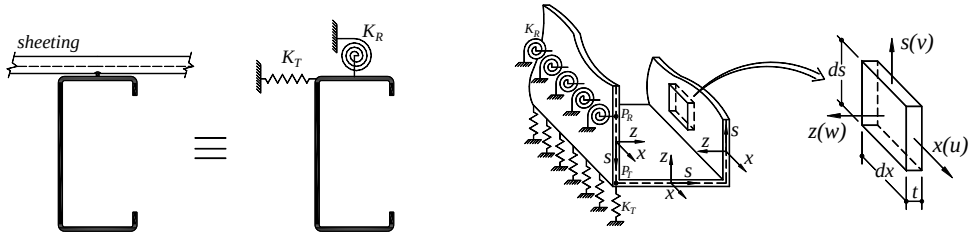

(a) (b)

Figure 22: Prismatic thin-walled member (a) with continuous elastic restraints/springs and (b) local coordinate axes

The equations providing the member buckling behavior, taking into account the presence of elastic constraints (springs), are obtained by imposing the stationarity of the total potential energy functional

$$V = \frac{1}{2}\int_{\Omega} \sigma_{ij}\varepsilon_{ij}\, d\Omega + \frac{1}{2}\int_{L} K\Delta_r^2\, dx \tag{7}$$

in the close vicinity of the member fundamental equilibrium path (adjacent equilibrium) – (i) Ω is the member volume (n walls), (ii) σ_{ij} and ε_{ij} are the second Piola-Kirchhoff stress and Green-Lagrange strain tensors, respectively, both comprising pre-buckling and bifurcated components, (iii) L is the member length, (iv) K is the stiffness of a continuous (along a longitudinal axis r) spring, (v) Δ are spring generalised displacements (translation or rotation) and (vi) the summation convention applies to subscripts i and j. Then, the equilibrium equations defining the member buckling eigenvalue problem are obtained by (i) linearising the first variation (δ) of the total potential energy functional, at the fundamental equilibrium path, and (ii) discarding the pre-buckling strains (*e.g.*, Camotim *et al.* 2008), thus yielding (*e.g.*, for members subjected to uniform internal forces and moments)

$$\delta V = \int_L \left(C_{ik}\phi_{k,xx}\delta\phi_{i,xx} + D_{ik}^1\phi_{k,x}\delta\phi_{i,x} + D_{ik}^2\phi_k\delta\phi_{i,xx} + D_{ki}^2\phi_{k,xx}\delta\phi_i + B_{ik}\phi_k\delta\phi_i + \lambda W_j^0 X_{jik}^{\sigma-x}\phi_{k,x}\delta\phi_{i,x} \right) dx = 0 \tag{8}$$

with

$$C_{ik} = E\int_b t\, u_i u_k\, ds + \frac{E}{12(1-\upsilon^2)}\int_b t^3\, w_i w_k\, ds \tag{9}$$

$$B_{ik} = \frac{E}{12(1-\upsilon^2)}\int_b t^3\, w_{i,ss} w_{k,ss}\, ds + K_T w_i(s_{P_T}) w_j(s_{P_T}) + K_R w_{i,s}(s_{P_T}) w_{j,s}(s_{P_T}) \tag{10}$$

$$D_{ik}^1 = \frac{G}{3}\int_b t^3\, w_{i,s} w_{k,s}\, ds \qquad\qquad D_{ik}^2 = \frac{\upsilon E}{12(1-\upsilon^2)}\int_b t^3\, w_i w_{k,ss}\, ds \tag{11}$$

$$X_{jik}^{\sigma-x} = \frac{E}{C_{jj}} \int_b t\, u_j (v_i v_k + w_i w_k) ds \tag{12}$$

where E, υ and G are the material Young's modulus, Poisson's ratio and shear modulus.

Once the displacement field components ($u_k(s)$, $v_k(s)$, $w_k(s)$) are known, it is possible to calculate the matrices $[C_{ik}]$, $[D_{ik}]$, $[B_{ik}]$ and $[X_{ik}]_j$ appearing in system (2), which constitutes a straightforward (but time/effort consuming) task. Moreover, it should be mentioned that all the above four matrices are fully populated, which means that system (2) is highly coupled, a fact that considerably complicates its solution and, more important than that, the interpretation of the results obtained. Indeed, the physical meaning of the various matrix components is far from obvious, even in the case of rather trivial and well-known phenomena (*e.g.*, bending). In order to take full advantage of all the GBT potential, mostly concerning the clarity and physical interpretation of the results, the above matrices must be rendered "as simple as possible", a goal achieved through the simultaneous diagonalization of matrices $[C_{ik}]$ and $[B_{ik}]$, whose process is described in detail in da Silva *et al*. 2019).

5.2 Illustrative Examples

This section presents and discusses numerical results concerning the buckling behaviour of cold-formed steel ($E=210GPa$ and $\upsilon=0.3$) purlins restrained by sheeting. Figure 23(a) shows the dimensions of the lipped channel cross-section of two purlins, which are continuously restrained by rotational (K_R) and translational (K_T) springs with different stiffness values (*Constraints I* and *II*). For each of them, Figure 23(b) displays the *8* most relevant deformation modes obtained by means of the proposed restrained cross-section analysis procedure (mode **1** stands for axial extension) – for comparison purposes, Figure 24 depicts the first *9* (conventional) deformation modes yielded by code GBTUL2.0 for an unrestrained lipped channel cross-section. Table 2 show the components of the $[C_{ik}]$ (diagonal), $[B_{ik}]$ (diagonal) and $[D_{ik}]$ (almost diagonal) stiffness matrices concerning deformations modes **2** to **9** of unrestrained and with *Constraint I*. Note that the *Constraint I* only does not restrain mode **2** – thus, C_{22} B_{22} and D_{22} are equal for the sections unrestrained and restrained. Moreover, matrix D_{ik} tends to be "less diagonal" as the restraints. Finally, the local modes (**7**, **8** and **9**) are very little affected by the restrictions.

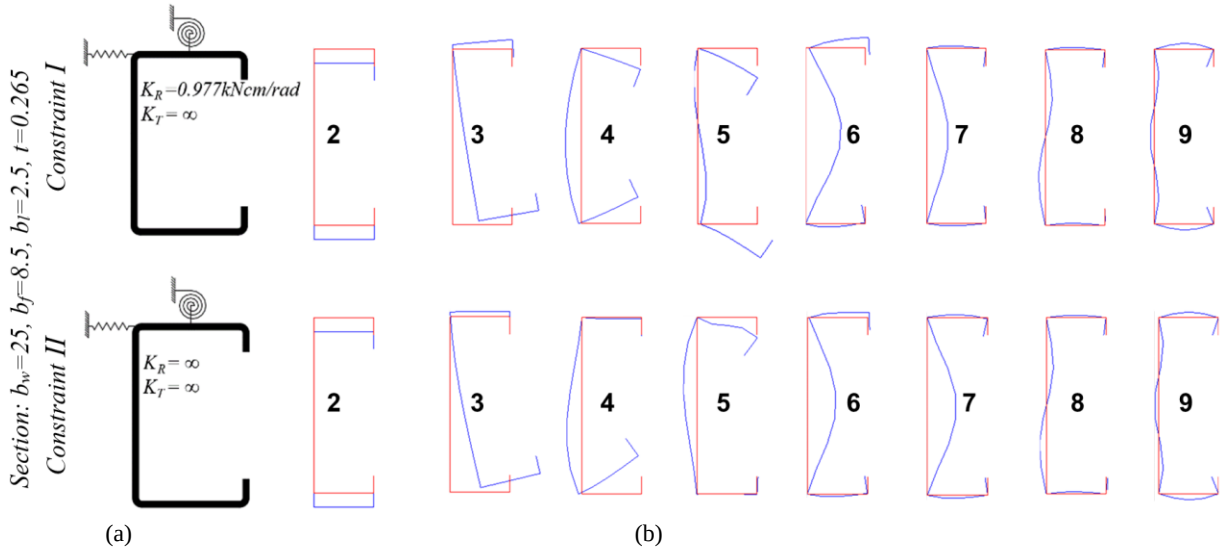

Figure 23: (a) Restrained lipped channel cross-sections and (b) *8* most relevant deformation modes for each of them

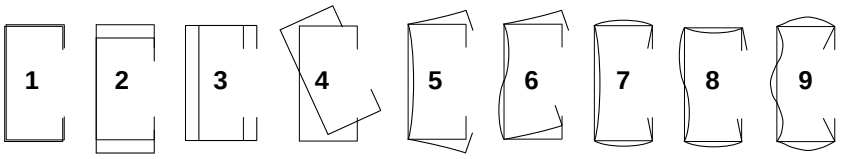

Figure 24: Main features of the most relevant conventional lipped channel deformation modes yielded by GBTUL2.0

Table 2: Components of C_{kk}, B_{kk} and D_{ik} stiffness matrices concerning modes **2-9** for unrestrained and restrained, by *Constraint I*, lipped channel cross-sections – dimensions in *cm*, Young and shear moduli in kN/cm^2

Unrestrained Section (GBTUL2.0) - $C_{kk} \times 10^4$							
2556	327.3	35163	1.038	1.135	0.043	0.047	0.048

Constraint I - $C_{kk} \times 10^4$							
2556	2.797	1.013	0.905	0.594	0.046	0.047	0.048

Unrestrained Section (GBTUL2.0) - $B_{kk} \times 10^{-2}$							
0	0	0	1.789	5.103	31.62	278.8	858.7

Constraint I - $B_{kk} \times 10^{-2}$							
0	0.004	2.162	3.625	374.4	34.16	278.9	856.9

Unrestrained Section (GBTUL2.0) - D_{ik}							
0	0	0	0	-0.919	0	-6.078	0
0	0	0	-1.085	0	-1.431	0	-6.854
0	0	2355	0	53.01	0	32.01	0
0	-1.085	0	5.927	0	3.966	0	-2.714
-0.919	0	53.01	0	5.962	0	-3.279	0
0	-1.431	0	3.966	0	15.65	0	4.966
-6.078	0	32.01	0	-3.279	0	68.95	0
0	-6.854	0	-2.714	0	4.966	0	158.2

Constraint I - D_{ik}							
0	0	0.106	-0.715	-0.261	-0.018	6.083	-0.019
0	0.0764	-0.083	0.224	0.035	0	-0.222	0.587
0.106	-0.083	5.114	-0.817	4.395	-3.612	-0.430	-2.657
-0.715	0.224	-0.817	3.738	1.262	0.315	2.480	-0.045
-0.261	0.035	4.395	1.262	14.54	-14.51	1.815	3.911
-0.018	0	-3.612	0.315	-14.51	15.70	0.127	-5.019
6.083	-0.222	-0.430	2.480	1.815	0.127	68.97	0
-0.019	0.587	-2.657	-0.045	3.911	-5.019	0	157.8

Attention is turned next to simply supported steel purlins restrained by steel sheeting and subjected to uniform *negative* major-axis bending (bottom flange under compression) – the sheeting restraints are modelled through *Constraint II* with fully prevented translation and rotation (springs with infinite stiffness). Figure 25 shows the signature curves of the unrestrained ($K_R=K_T=0$) and fully restrained ($K_R=K_T=\infty$) purlins, providing the variation of the critical buckling moment M_{cr} and mode shape with the length L (logarithmic scale) – the buckling mode half-wave numbers are inside brackets. Besides the results obtained through restrained-mode GBT analyses (solid and dashed curves, and buckling mode shapes), the figure also display, for validation and comparison purposes, some critical buckling moment determined by means of GBTUL2.0 analyses (circles) – all analyses adopt longitudinal discretizations into *10* finite elements and include all deformation modes. The close observation of the buckling results displayed in this figure prompts the following remarks:

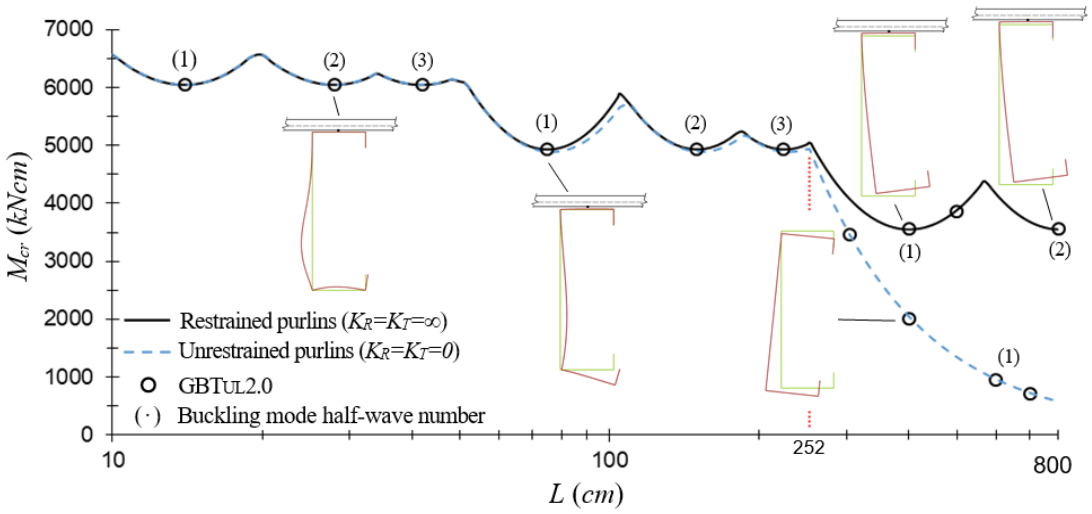

Figure 25: Variation of the critical buckling moment and mode shape with the purlin length

(i) As before, the buckling moments provided by GBTUL2.0 and those obtained with the proposed formulation virtually coincide (all differences are below 1.0%).

(ii) For $L \leq 252$ *cm*, the buckling behaviour does not depend on the restraint conditions (the solid and dashed curves coincide). This is because the critical buckling modes combine local and/or distortional deformations that do not involve upper flange horizontal displacements or rotations.

(iii) In the restrained purlins with $L > 252$ *cm*, the buckling mode shape is clearly lateral-distortional, due to the full restraint of the upper flange horizontal displacements and (mostly) rotations – this instability phenomenon has also been investigated by other authors (*e.g.*, Hancock *et al.* 2001).

(iv) In the unrestrained purlins with $L > 252$ *cm*, lateral-torsional buckling occurs and is associated with a very pronounced M_{cr} decrease. As shown by Basaglia *et al.* (2013), there is a minute horizontal displacement of the point where the translational restraint is located – see the buckling mode shape of the unrestrained purlin with $L=400$ *cm*.

Finally, for a few purlins buckling in distortional or lateral-distortional modes, Table 3 provides the critical buckling moments obtained by means of GBT analyses including all deformation modes and also either only the dominant ("restrained GBT") or the two most relevant (GBTUL2.0) ones. It is observed that, once again, the GBT analyses including a single restrained deformation mode (**3** or **4** – see Fig. 23(b)) provide accurate buckling moments. Conversely, the inclusion of the two most relevant deformation modes in the GBTUL2.0 analyses still leads to inaccurate buckling moments.

Table 3: Purlin buckling results: GBT (GBTUL2.0 and restrained deformation modes) analyses

L (cm)	Conventional Modes (GBTUL2.0)					Restrained Modes				
	All Modes		Two Modes		Δ (%)	All Modes		Single Mode		Δ (%)
	Mcr (kNcm)	Modal Participations	Mcr (kNcm)	Modes	Two / All	Mcr (kNcm)	Modal Participations	Mcr (kNcm)	Mode	Single / All
75	4933.78	52%**(6)** + 47%**(5)** + 1%	8608.13	(6)+(5)	74.5	4933.88	95%**(4)** + 1.1%(3) + 3.9%	5028.73	(4)	1.9
150	4934.20	52%**(6)** + 47%**(5)** + 1%	8235.79	(6)+(5)	66.9	4934.30	95%**(4)** + 1.1%(3) + 3.9%	5029.17	(4)	1.9
224	4936.10	52%**(6)** + 47%**(5)** + 1%	7870.98	(6)+(5)	59.5	4936.19	95%**(4)** + 1.1%(3) + 3.9%	5031.76	(4)	1.9
400	3551.75	52%**(3)** + 47**(4)** + 1%	71389.38	(3)+(4)	1910.0	3554.28	99.5%**(3)** + 0.5%	3566.53	(3)	0.3
500	3863.29	52%**(3)** + 47**(4)** + 1%	71510.10	(3)+(4)	1751.0	3867.27	99.4%**(3)** + 0.6%	3888.06	(3)	0.5
800	3552.10	52%**(3)** + 47**(4)** + 1%	72237.60	(3)+(4)	1933.7	3554.63	99.5%**(3)** + 0.5%	3566.88	(3)	0.3

6. Conclusions

This paper presented and discussed numerical results dealing with the application of GBT-based beam finite element models to analyze the buckling behavior of four thin-walled steel structural systems, namely locally and globally braced frames, pitched-roof industrial frames, roof-supporting trusses and purlins restrained by sheeting, exhibiting different support conditions and subjected to various loadings. These numerical results provided ample evidence of the enormous capabilities and potential of the GBT unique modal approach to structural analysis, particularly in terms of (i) numerical efficiency (the numbers of degrees of freedom involved are quite small – orders of magnitude apart from those required by similarly accurate shell finite element analyses) and, mostly, (ii) acquisition of in-depth insight on the mechanics of the instability phenomenon under consideration.

Initially, GBT analyses were employed to make an in-depth assessment of the influence and effectiveness of bracing arrangements on the local and global buckling behavior of thin-walled steel frames – in this particular case, they caused (i) critical buckling load increases ranging from *69%* to *287%* and (ii) significant changes in the buckling mode shape nature. Then, attention was devoted to the influence of the elastic restraints provided by the purlin/sheeting systems on the buckling behavior of pitched-roof steel frames built from I-section members and acted by evenly spaced vertical point loads Q, transferred to the rafters through the purlins. Next, the local and global buckling behavior of

plane trusses formed by plain channel chords and diagonals connected by pinned joints were investigated – depending on the truss geometry, its instability was triggered by either chord local buckling or diagonal global buckling. Finally, the paper closed presenting the application of a novel GBT formulation for the local, distortional and global buckling analysis of purlins restrained by sheeting, based on a cross-section analysis procedure that incorporates elastic restraints and, therefore, is capable of providing accurate buckling results with a single deformation mode, which enables the development of analytical formulae to calculate critical buckling loadings of restrained members – this feature, currently being exploited by the authors, will be addressed in future works. For comparison and illustration purposes, buckling results yielded by ANSYS shell finite element analyses were also included in the paper. Despite the disparity in the numbers of degrees of freedom involved, the critical buckling loads and mode shapes provided by the GBT and ANSYS analyses were shown to virtually coincide in all cases, thus confirming the numerical efficiency of the GBT-based beam finite elements. Moreover, it was clearly illustrated that the mechanical insight provided by the GBT modal solutions cannot be achieved by the ANSYS shell finite element results.

Final Remarks and Acknowledgments

This paper provides the content of the "MAJR Medal Presentation" delivered by the first author, who would like to express his most sincere gratitude to Professor Dinar Camotim (second author) for the scientific guidance during almost 15 years of continuous research cooperation and, most of all, for the invaluable friendship that will endure for the rest of our lives. Special thanks are also due to our "fellow GBT researchers" at the University of Lisbon, for their help and camaraderie.

References

Basaglia C, Camotim D (2011). GBT-based buckling analysis of cold-formed steel trusses, *Proceedings of 6th International Conference on Thin-Walled Structures – Recent Research Advances and Trends* (ICTWS - Timisoara, 5-7/9), D. Dubina, V. Ungureanu (Eds.), ECCS (Brussels), vol. 1, 149-156.

Basaglia C, Camotim D (2013). Enhanced generalised beam theory buckling formulation to handle transverse load application effects, *International Journal of Solids and Structures*, **50**(3-4), 531-547.

Basaglia C, Camotim D (2015). Buckling Analysis of Thin-Walled Steel Structural Systems Using Generalized Beam Theory (GBT), *International Journal of Structural Stability and Dynamics*, **15**(1), 1540004-1 - 1540004-28.

Basaglia C, Malite M, Munaiar Neto J, Gonçalves RM (2005). Stability of steel purlins under wind uplift considering the purlin-sheeting behaviour, *Proceedings of fourth European conference on steel and composite structures* (Eurosteel - Maastricht, 8-10/6), B Hoffmeister, O Hechler (Eds.), 1.4.41-7.

Basaglia C, Camotim D, Silvestre N (2008). Global buckling analysis of plane and space thin-walled frames in the context of GBT, *Thin-Walled Structures*, **46**(1), 79-101.

Basaglia C, Camotim D, Silvestre N (2009a). Buckling Behaviour of Locally and Globally Braced Thin-Walled Frames, *Proceedings of Sixth International Conference on Advances in Steel Structures* (ICASS - Hong Kong, 16-18/12), S.L. Chan (Ed.), 891-898.

Basaglia C, Camotim D, Silvestre N (2009b), GBT-based local, distortional and global buckling analysis of thin-walled steel frames, *Thin-Walled Structures*, **47**(11), 1246-1264.

Basaglia C, Camotim D, Silvestre N (2010). GBT-Based Buckling Analysis of Thin-Walled Steel Frames with Arbitrary Loading and Support Conditions, *International Journal of Structural Stability and Dynamics*, **10**(3), 263-85.

Basaglia C, Camotim D, Gonçalves R, Graça A (2013). GBT-Based Assessment of the Buckling Behaviour of Cold-Formed Steel Purlins Restrained by Sheeting, *Thin-Walled Structures*, **72**(November), 217-219.

Basaglia C, Camotim D, Silvestre N (2015). Buckling and vibration analysis of cold-formed steel CHS members and frames using generalized beam theory, *International Journal of Structural Stability and Dynamics*, **15**(8), 1540021-1 - 1540021-25.

Bebiano R, Gonçalves R, Camotim D (2015). A cross-section analysis procedure to rationalise and automate the performance of GBT-based structural analyses, *Thin-Walled Structures*, **92**(July), 29-47.

Bebiano R, Basaglia C, Camotim D, Gonçalves R (2018). GBT buckling analysis of generally loaded thin-walled members with arbitrary flat-walled cross-sections, *Thin-Walled Structures*, **123**(February), 11-24.

Camotim D, Basaglia C (2013). Buckling analysis of thin-walled structures using Generalised Beam Theory (GBT): state-of-the-art report, *Steel Construction*, **6**(2), 117-131.

Camotim D, Basaglia C (2014). On the behaviour, failure and direct strength design of thin-walled steel structural systems, *Thin-Walled Structures*, **81**(August), 50-66.

Camotim D, Silvestre N, Basaglia C, Bebiano R (2008). GBT-based buckling analysis of thin-walled members with non-standard support conditions. *Thin-Walled Structures*, **46**(7-9), 800-815.

Camotim D, Basaglia C, Silvestre N (2010). GBT buckling analysis of thin-walled steel frames: a state-of-the-art report, *Thin-Walled Structures***, 48**(10-11), 726-743.

da Silva TG, Basaglia C, Camotim D (2019). On the incorporation of cross-section restraints in Generalised Beam Theory (GBT), *Proceedings of the 2019 International Colloquia on Stability and Ductility of Steel Structures* (SDSS - Prague, 11-13/9), F. Wald, M Jandera (Eds.), CRC Press: Taylor & Francis Group, 1015-1024.

Davies JM (1991). Sheeting and decking, *Design of Cold-Formed Steel Members*, J. Rhodes (Ed.), Elsevier Applied Science, New York, 339-360.

Dubina D (2008). Structural analysis and design assisted by testing of cold-formed steel structures, *Thin-Walled Structures*, **46**(7-9) 741-764.

Hancock GJ, Murray TM, Ellifritt DS (2001). *Cold-Formed Steel Structures to the AISI Specification*, Marcel Dekker Inc., New York.

Jakab G (2009). *Analysis and Design of Cold-Formed C-Section Members and Structures*, Ph.D. Thesis, University of Technology and Economics, Budapest, Hungary.

Jiang C, Davies JM (1997). Design of thin-walled purlins for distortional buckling, *Thin-Walled Structures* **29**(1-4), 189-202.

SAS (Swanson Analysis Systems Inc.) (2013). *ANSYS Reference Manual* (version 15).

Schardt R (1989). *Verallgemeinerte Technishe Biegetheorie*, Springer-Verlag, Berlin. (German)

Tomà A, Sedlacek G, Weynand K (1993). Connections in cold-formed steel, *Thin-Walled Structures*, **16**(1-4), 219-237.